Enhanced adsorption performance of methylene blue from aqueous solutions onto modified adsorbents prepared from sewage sludge

Tao Chen, Bo Yan, Da-Mao Xu and Li-li Li

ABSTRACT

In the present work, an attractive and creative adsorbent derived from sewage sludge was freshly fabricated via pyrolysis technology, followed by modification for improving the absorptive ability. First, the $(NH_4)_2S_2O_8$ modified pyrolytic sludge (MS_{AP}) was selected from 19 modified pyrolytic sludges for the highest removal efficiency and adsorption capacity for methylene blue (MB). Then, the adsorption performance for MB of MS_{AP} was compared systematically with the pristine adsorbent (MS_{DW}) by batch adsorption experiments. The main conclusions were that the adsorption process was better fitted with the Langmuir model, and the maximum adsorption capacity (q_{max}) of MS_{AP} was observed to be 149.05 mg g^{-1}. Moreover, the adsorption kinetics data showed a good fit with the pseudo second order model; when the addition of MS_{AP} was 1.0 g·L^{-1}, the rate constant was 0.05 g·mg^{-1}·min^{-1}, which was far greater than that of the other modified adsorbents.

Key words | adsorption performance, methylene blue (MB), pseudo second order model, sewage sludge modification

Tao Chen
Bo Yan (corresponding author)
The Environmental Research Institute; MOE Key Laboratory of Theoretical Chemistry of Environment,
South China Normal University,
Guangzhou 510006,
China
E-mail: *yanbo2007@gig.ac.cn*

Da-Mao Xu
Li-li Li
State Key Laboratory of Organic Geochemistry,
Guangzhou Institute of Geochemistry,
Chinese Academy of Sciences,
Guangzhou 510640,
China

Da-Mao Xu
University of Chinese Academy of Sciences,
Beijing 100082,
China

NOMENCLATURE

MB	Methylene blue.
SS	Sewage sludge that has been dehydrated at ambient temperature.
PS	Pyrolytic sludge: the pyrolysis occurred in a muffle furnace, the final temperature was 800 °C, and the pyrolytic process took 3 h.
MS_x	The modified product of the PS, where x represents the used modifier.
Distilled water	DW; SA: H_2SO_4; PA: H_3PO_4; SH: NaOH; SC: NaCl; SCB: Na_2CO_3; AC: NH_4Cl; ZC: $ZnCl_2$; FC: $FeCl_3$; FS: $Fe_2(SO_4)_3$; HP: H_2O_2; AP: $(NH_4)_2S_2O_8$; CTMAB: $C_{19}H_{42}BrN$; SDB: $C_{18}H_{29}NaO_3S$; SDS: $C_{12}H_{25}SO_3Na$; MB: $C_{16}H_{18}N_3SCl$.
$MS_{X/MV}$	represents MB_X that has been further modified with microwaves.
$MS_{X/US}$	represents MB_X that has undergone ultrasound-assisted modification.

INTRODUCTION

Synthetic dyes are highly notorious compounds in wastewater, for which there is an increasing demand in diversified fields, mainly industrial operations involved in textiles, dyestuffs, cosmetics and so on (Zhang *et al.* 2017). The worldwide concern regarding dyes in wastewater is that they have adverse and detrimental outcomes toward ecological environments (Manna *et al.* 2017). Consequently, it is industrially imperative to develop effective, convenient and economical approaches for the removal of excess synthetic dyes prior to discharge into natural water bodies (Luo *et al.* 2017). Methylene blue (MB) ($C_{16}H_{18}N_3SCl$; molecular weight: 319.85 g·mol^{-1}), as a typical example of a thiazine cationic dye, is extensively utilized (Miraboutalebi *et al.* 2017). The existence of this contaminant in aquatic systems, even at minuscule concentrations (less than 1 ppm), has been demonstrated to bring about severe health hazards for human beings and animals. Therefore, MB has been widely used as an adsorbate molecule for

doi: 10.2166/wst.2018.351

the testing of adsorbents in adsorption studies (Rashed *et al.* 2016).

Various traditional treatment methods for the eradication and elimination of waterborne dyes from wastewater sources, including coagulation, chemical precipitation, ion exchange, electrochemical destruction and membrane filtration, have been commonly researched and implemented in recent decades (Chen *et al.* 2015). However, there are some drawbacks such as high handling cost, incomplete removal and the fact that the processes are highly energy intensive. Among these proposed methods, adsorption techniques have been routinely recognized as the most preferred alternative due to their low operational costs, easy engineering applications and superior environmental properties in the de-coloration process (Qin *et al.* 2018). More recently, to bypass those critical shortcomings, that commercial adsorbents are non-renewable and relatively expensive for the disposal of dyeing effluents, much effort has been devoted to innovatively introducing extraordinary performance and environmentally friendly adsorbents, produced from natural materials or industrial wastes, holding more remarkable features and linked to abundant reserves (Jung *et al.* 2016). Large volumes of sewage sludge (SS), generated as a by-product of the municipal and industrial wastewater treatment process, can be converted to an attractive adsorbent for the treatment of dye-containing wastewaters due to its unparalleled physico-chemical properties (Rashed *et al.* 2016). Nevertheless, the general adsorption performance of pyrolytic sludge (PS) is definitely far from meeting the needs of commercial applications. These sludges usually suffer from slow adsorption or limited adsorption capacity, probably due to the high ash content. To the best of our knowledge, there is little available literature that has made an attempt to modify the PS via methods such as chemical and ultrasonic or microwave energy-assisted modification, which would make great contributions toward improving its adsorption characteristics.

Thus, the preparation and modification of prospective adsorbents based on PS were undertaken for the adsorption of MB from simulated wastewater. The principal concepts of environmentally critical importance to be considered are as follows: (i) the insights regarding the adsorption performance of pristine and modified adsorbent were fully revealed for comparison purposes; (ii) tests were conducted to systematically depict the adsorption characterizations by evaluating the effects of independent variables such as initial pH, initial concentration, temperature and contact time; (iii) the adsorption mechanisms were thoroughly elucidated.

MATERIALS AND METHODS

Preparation and modification of adsorbent

Dehydrated SS, employed for the production of the precursor material, was collected locally from the Li-jiao Municipal Sewage Treatment Plant located in Guangzhou, southern China. Adsorbents derived from SS were produced by pyrolysis technology in accordance with the procedures described in detail by these previous works (Ferreira *et al.* 2017). The PS was washed with plenty of distilled water to remove soluble impurities until the pH reached a constant value, whereupon the washed PS was dried at 105 °C in an oven to constant weight and then retained in a clean, dry desiccator for further use.

To address the abovementioned disadvantages, suitable strategies have been devised and are proposed by our research group for this purpose: (A) chemical modification of the adsorbent surface through loading of inorganic ions; (B) chemical grafting of new functional groups onto the surface of the adsorbent; (C) oxidation, provoking the explosive properties of the adsorbent surface; (D) ultrasonic (US) or microwave (MW) energy assisted modification to tailor the surface properties of the adsorbent.

To modify the PS by loading with inorganic ions, two typical inorganic acids have been used. One typical alkaline and six typical inorganic salts were selected. When the SA, PA, and SA solutions were used for the modification, the PS was dissolved in the 5% solution, and then the suspensions were put into a muffle furnace and calcined at 65 °C for 6 h. Next, the obtained mixtures were filtered and then washed to neutral with distilled water. Six typical inorganic salts were used for the modification of the PS; the PS was then separately soaked for 6 h in saturated salt solutions of sodium chloride (SC), sodium carbonate (SCB), ammonium chloride (AC), zinc chloride (ZC), ferric chloride (FC) and ferric sulfate (FS) without pH adjustment under stirring, and the resultant suspensions were recovered by centrifugation before being filtered and washed with distilled water thoroughly.

Cetrimonium bromide (CTMAB), sodium dodecyl sulfonate (SDS), and sodium dodecylbenzenesulfonate (SDB) were employed for the chemical grafting of new functional groups onto the surface of the adsorbent. The PS was dispersed with CTMAB, SDS, and SDB solutions and then stirred for 6 h. Then, the resulting solids were separated by centrifugation and washed with distilled water thoroughly.

Ammonium persulfate (AP) solution and hydrogen peroxide (HP) solution were employed for the oxidative

modification of the PS. The resulting solids were washed with distilled water until the filtrate pH was neutral.

Four modified PS samples were treated with 500-W microwaves for 10 min at room temperature for their further modification.

$MS_{CTMAB/US}$ was obtained by ultrasound assisted modification (frequency: 40 KHz, power: 300 W). Subsequently, the treated sample was centrifuged at 4,500 rpm for 10 min, harvested by filtration, and washed with distilled water.

All of the abovementioned modified PS adsorbents were rinsed with distilled water and further dried to constant weight at 105 °C.

Analytical methods and characterization techniques

Proximate analysis data (moisture, volatile matter, ash and fixed carbon) were acquired by the method for the proximate analysis of coal. The ash composition was determined by X-ray fluorescence spectroscopy (XRF1800, Shimadzu, Japan). All solution pH values were monitored using a digital pH meter (pH-3C, Lei-ci, China). The MB concentration was detected by ultraviolet spectrophotometry (UV1800, Shimadzu). The morphological structure of the as-fabricated products was visualized with scanning electron microscopy (SEM) operated at 3 kV accelerating voltage (S-4800, Hitachi, Japan). Energy dispersive X-ray spectroscopy (EDX) analysis was performed to determine the elemental composition. Fourier transform infrared spectroscopy (FT-IR) was obtained using a Bruker VERTEX 70 Fourier transform infrared spectrometer (Bruker, Germany) with the KBr pressed pellet method. The surface area and porosity were obtained using the ASAP 2020 Surface Area and Porosity Analyzer (Micromeritics, USA).

Batch adsorption procedure

Exact amounts of dried MS were added into 100 mL of solution containing certain MB concentrations in a series of 250 mL stoppered Erlenmeyer flasks, which were then oscillated on a reciprocating water-bath shaker operated at a constant speed of 220 rpm·min^{-1} to ensure their full contact. The contact time for the adsorption of MB by both MS_{DW} and MS_{AP} was set according to test requirements, and these were listed in the batch adsorption process. After that, the homogeneous suspensions were separated via centrifugation at 4,000 rpm for 20 min and were then filtered off with 0.45-μm membrane filters.

The dye removal efficiency (expressed as RE, %) and the amount of dye adsorbed onto the adsorbent (expressed as q, mg·g^{-1}) were calculated using Equations (1) and (2), respectively:

$$\mathrm{RE} = \frac{(C_0 - C_e)}{C_0} \times 100\% \quad (1)$$

$$q_t = \frac{(C_0 - C_e)V}{M} \quad (2)$$

where

RE is the removal efficiency, %;

C_0 and C_e represent the concentration present in the initial and the final liquids, respectively, mg·L^{-1};

q_t is the amount of dye adsorbed by the adsorbent, mg·g^{-1};

V is the volume of the solution, L;

M is the mass of the adsorbent kept in contact with the solution, g.

RESULTS AND DISCUSSION

Selection of the best modified adsorbent for MB adsorption

The effectiveness of the MS_x with the different types of modifiers in the adsorption of MB was evaluated under the following conditions: the initial concentration of MB was 50 mg·L^{-1}, the initial pH was set as 10, the dosage of MS_x was 0.5 g·L^{-1}, and the time was 5 min. The obtained results are depicted in Figure 1. The maximum removal efficiency and adsorption capacity of MS_{AP} were observed to be 96.18% and 96.80 mg·g^{-1}, respectively. The RE of MS_{AP} was 1.2 to 4.4 times that of the other types of MS_x, and it was 2.4 times that of the PS (MS_{DW}). Hereinafter, MS_{AP} has been selected as the highly representative adsorbent.

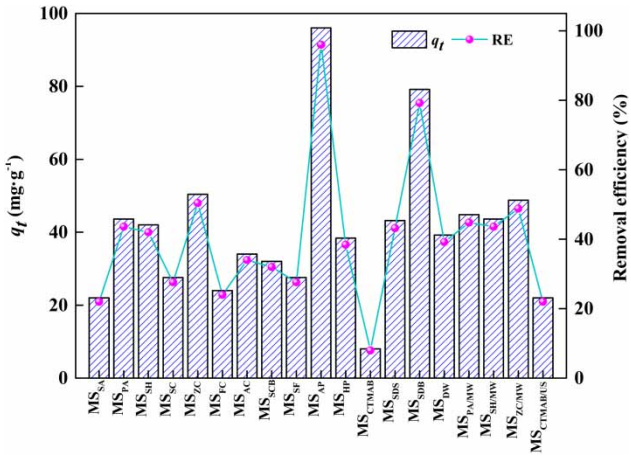

Figure 1 | Comparison of adsorption performance among various modified MS.

From the SEM micrographs shown in Figure 2(a) and 2(c), the rough surface of MS_{DW} appeared relatively more irregular and aggregate in comparison to the smooth surface of MS_{AP}. Additionally, such morphological architectures with a high density of scattered and disordered holes uniformly distributed on the outer surface of MS_{AP} were clearly observed in Figure 2(d), which were significantly different from those of MS_{DW}, as shown in Figure 2(b).

This difference was probably due to the sufficient removal of surface impurities and amorphous constituents after the modification with the modifier $(NH_4)_2S_2O_8$. Additionally, it was reasonable to assume that oxidative reactions might have taken place between the modifier and the reduced spots on the starting materials in an acidic medium. As demonstrated in Table 1, the elemental analysis indicated that the percentages by atomic weight of elemental oxygen and sulfur on the surface of the modified MS_{AP} distinctly increased, but elemental carbon apparently decreased compared to the virgin MS_{DW}. This would be further indication that $(NH_4)_2S_2O_8$, as expected, had been loaded on the surface structure of MS_{DW} when forming MS_{AP}.

The results of the chemical analysis for the prepared samples are presented in Table 2. The volatile content increased drastically and moisture and fixed carbon contents increased slightly, whereas the ash exhibited a substantial decrease in the process of modification, which should be beneficial for the adsorption performances of the modified MS_{AP}. The chemical analysis data was indicative of the presence of impurities in the prepared sample. As also summarized in Table 2, the ash composition content in MS_{AP} remained distinctly unchanged apart from P_2O_5 (from 10.42% to 2.46%) and SiO_2 (from 51.22% to 60.35%), compared with those in MS_{DW}. Therefore, the high content of oxygen containing functional groups was imparted to the MS_{DW} as expected. It is likely that the preferable and superior adsorption ability of MS_{AP} was due to its characteristic features, that is, abundant reactive sites, large pore volume, and high surface area. With the analysis of surface area and porosity, it can be found that the Brunauer–Emmett–Teller (BET) specific surface area of MS_{AP} reached 484.09 $m^2 \cdot g^{-1}$, which was about four times the value of MS_{DW} (110.17 $m^2 \cdot g^{-1}$). Furthermore, the DA

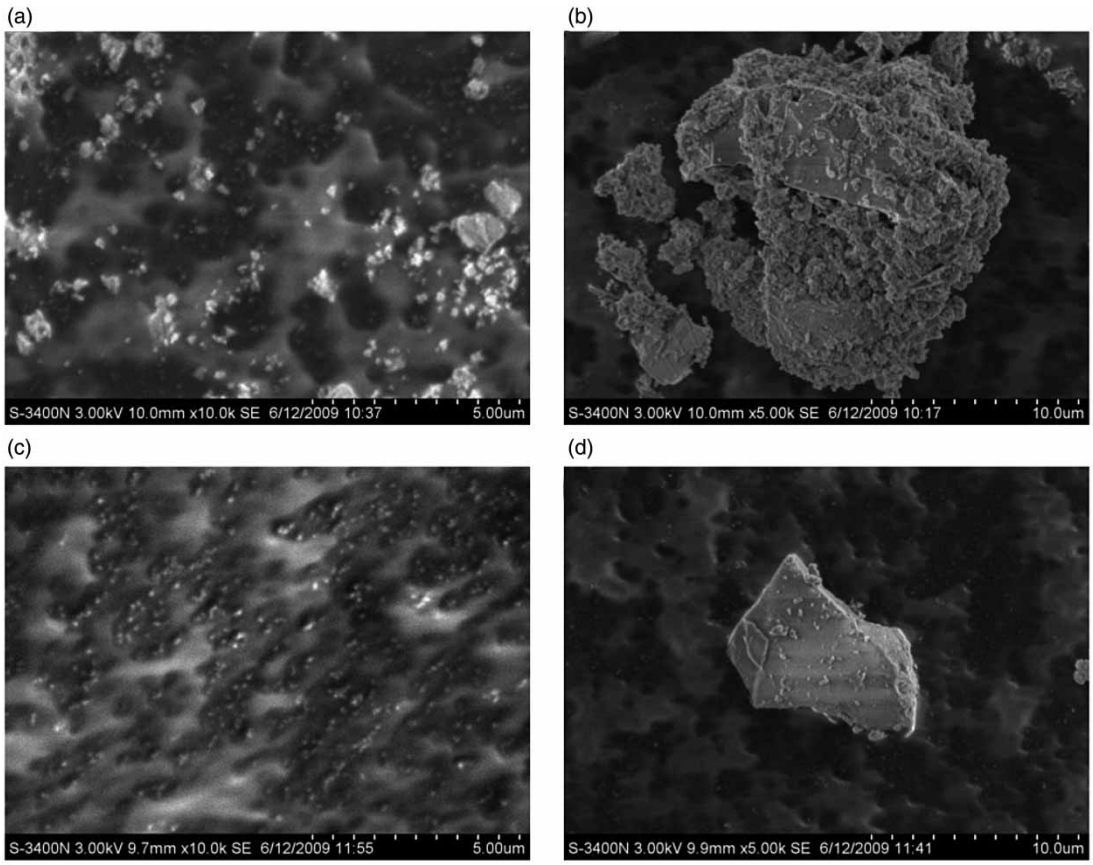

Figure 2 | SEM analysis of MS_{DW} (a) and (b) and MS_{AP} (c) and (d).

Table 1 | Elemental analysis of the MS_{DW} and MS_{AP} used in the present study

MS_{DW}	Elements	C	O	Na	Mg	Al	Si	P	S	K	Ca
	Wt (%)	9.30	46.70	0.21	0.51	10.05	5.69	10.81	0.23	0.44	3.85
	At (%)	15.57	59.68	0.19	0.43	7.49	4.07	7.02	0.14	0.23	1.93
MS_{AP}	Elements	C	O	Na	Mg	Al	Si	P	S	Cl	K
	Wt (%)	6.48	50.48	0.39	0.65	8.60	9.87	5.64	2.10	0.09	1.14
	At (%)	10.84	63.41	0.34	0.53	6.41	7.07	3.66	1.32	0.05	0.59
MS_{DW}	Elements	Ti	Cr	Mn	Fe	Co	Ni	Cu	Zn	Pb	
	Wt (%)	0.25	0.10	0.39	9.07	0.28	0.03	1.40	0.48	0.20	
	At (%)	0.10	0.04	0.14	3.26	0.10	0.01	0.44	0.15	0.02	
MS_{AP}	Elements	Ca	Ti	Cr	Mn	Fe	Ni	Cu	Zn	Pb	
	Wt (%)	4.32	0.89	0.12	0.48	6.26	0.25	1.87	0.24	0.12	
	At (%)	2.17	0.37	0.05	0.18	2.25	0.09	0.59	0.07	0.01	

Table 2 | Proximate and ash composition analysis

	Proximate analysis (wt %)				Ash composition analysis (%)									
Materials	**Moisture**	**Ash**	**Volatile**	**FC**	**Al_2O_3**	**CaO**	**Fe_2O_3**	**K_2O**	**MgO**	**MnO**	**Na_2O**	**P_2O_5**	**SiO_2**	**TiO_2**
MS_{DW}	5.5	48.8	43.8	2.32	18.41	3.59	7.97	3.93	2.72	0.06	0.78	10.42	51.22	0.92
MS_{AP}	7.58	36.27	49.72	6.43	16.9	1.08	8.75	3.9	0.9	0.03	0.91	2.46	60.35	1.09

micropore volume of MS_{AP} was reached 0.7353 $cm^3 \cdot g^{-1}$, which was about three times the value of MS_{DW} (0.2541 $cm^3 \cdot g^{-1}$).

Adsorption property studies

The simultaneous adsorption of MB was further investigated by batch techniques, together with that of the MS_{DW} for quantitative comparison. The comprehensive influences of various parameters were examined; namely, solution pH (between 2 and 11), initial concentration (between 25 and 300 $mg \cdot L^{-1}$), adsorbent doses (between 0.25 and 1 $g \cdot L^{-1}$), temperature (between 20 °C and 40 °C) and contact time (between 1 and 30 min).

The effect of initial pH on adsorption

The impact of pH variations was investigated first, since pH is an essential and crucial parameter that may influence not only the surface charge of the adsorbent but also the forms of adsorbate that exist in solution (Banaei *et al.* 2017). As an important part of this study, the pH-dependent adsorption experiments with both MS_{DW} and MS_{AP} towards MB were tested with an initial concentration of 50 $mg \cdot L^{-1}$ at 30 °C for 5 min, while the dosage of adsorbents was 0.5 $g \cdot L^{-1}$. The initial pH levels of the MB solutions were carefully adjusted between 2.0 and 11.0 by adding either 0.1 $mol \cdot L^{-1}$ HCl or NaOH solution (Fan *et al.* 2016). A graph was therefore relevantly plotted with the adsorption performance of MS_{DW} and MS_{AP} against initial pH of the experimental solutions over a wide range from 2 to 11 (Figure 3).

It can be concluded from Figure 3 that the MB adsorption was evidently pH-dependent, which gave the useful information that the electrostatic interaction played an important role in the control of the adsorption process of MB onto both MS_{DW} and MS_{AP}. As clearly evidenced by the steeper slope in Figure 3, there was little difference between MS_{DW} and MS_{AP} in the variation tendency of q_e and RE irrespective of the solution pH. It is worth pointing out that when the pH was increased to 10, the highest q_t and RE for MS_{DW} were 39.60 $mg \cdot g^{-1}$ and 39.46%, respectively. In comparison, MS_{AP} had maximum q_e and RE of 96.40 $mg \cdot g^{-1}$ and 96.40%, respectively.

At lower pH values, there exists an electrostatic repulsion between the positively charged surface of the adsorbent and the cationic MB molecules. The hydronium ion (H_3O^+) might generate competitive coordination with cationic MB molecules for their respective active sites, which would adversely lead to diminished MB adsorption onto the adsorbents. In contrast, as shown in Figure 4,

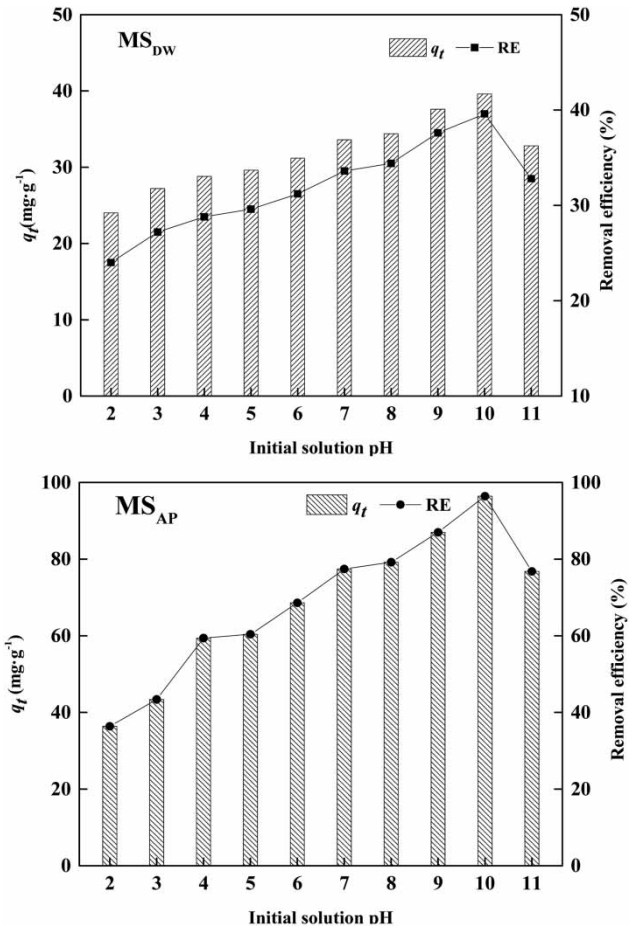

Figure 3 | Effect of pH on the adsorption of MB onto MS_{DW} and MS_{AP}.

when the pH was increased, the protonation was inhibited, and the electrostatic attraction was improved (Dahri *et al.* 2015), thus favorably resulting in a dramatically increased adsorption of MB onto the adsorbents. However, when the pH reached 11, the RE decreased for the decreased electrostatic attraction (Manna *et al.* 2017). As a result, the optimized pH of 10.0 was adopted for the rest of the adsorption experiments.

FT-IR analysis of MS_{AP} before and after MB adsorption was conducted (Figure 5). As presented in Figure 5, the broad absorption band at 3,423 cm^{-1} present both in MS_{AP} before and after adsorption is ascribed to the –OH stretching vibrations (Shim *et al.* 2014). The absorption band at 1,635 cm^{-1} appeared in MS_{AP} after the adsorption process, which is attributed to the symmetric stretching vibration of aromatic rings. The absorption band at 1,051 cm^{-1} is ascribed to the stretching vibration of C-S. It can be deduced that the adsorption of MB on MS_{AP} occurred and the H-bond and electrostatic interactions played an important role.

The BET specific surface area and the DA micropore volume of MS_{AP} after once adsorption process were 463.72 $m^2 \cdot g^{-1}$ and 0.7361 $cm^3 \cdot g^{-1}$, respectively. These values were almost unchanged compared with the raw MS_{AP}. The SEM of both fresh and MB loaded MS_{AP} are shown in Figure 6. There is evidence to suggest that the surface has been changed due to the biosorption of MB. It is also shown that the biosorbed MB tends to make the MS morphology structures less defined.

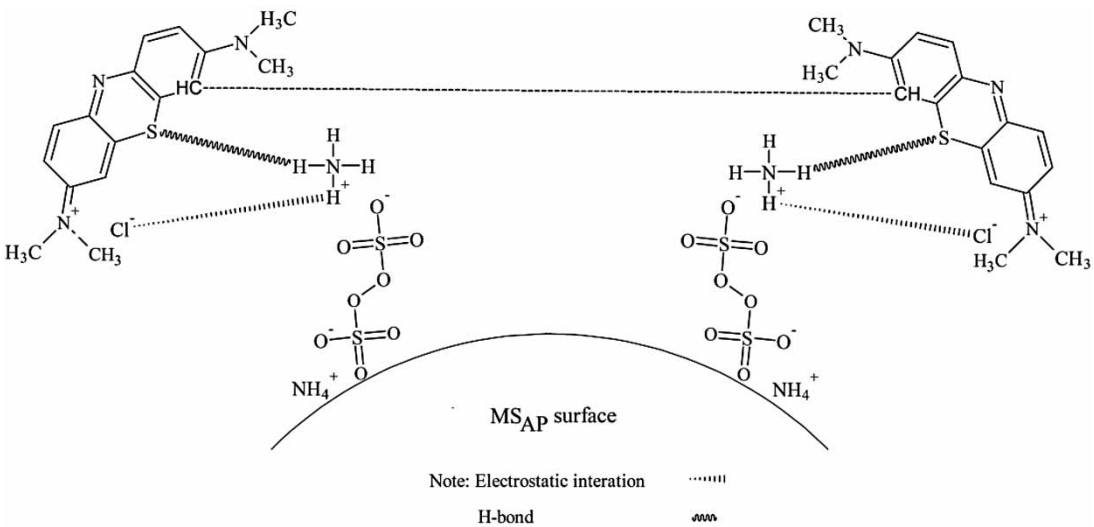

Figure 4 | Plausible mechanism for the adsorptive removal of MB by the adsorbent chemically modified with $(NH4)_2S_2O_8$ (MS_{AP}).

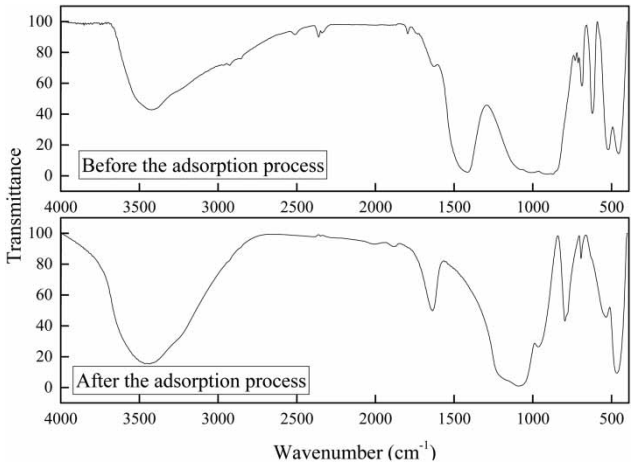

Figure 5 | FT-IR analysis for MS_{AP} before and after MB biosorption.

The effects of initial concentration and temperature

The plots of q_e and RE versus the initial MB concentration for MS_{DW} and MS_{AP} at three temperatures are displayed in Figure 7. The dosage of adsorbents was 0.5 g·L^{-1} and the reaction time was controlled at 5 min. When the initial MB concentration was increased from 25.0 mg·L^{-1} to 200.0 mg·L^{-1}, a rapid increase in q_e but an obvious decrease in RE of MS_{DW} and MS_{AP} towards MB were observed at fixed temperatures. However, when the initial MB concentration was increased beyond 200.0 mg·L^{-1}, there was little increase in RE. These results might arise from the approachability of vacant active sites for locating MB and the mass transfer driving force generated by the increased concentration gradient between the liquid and solid phases with an initial MB concentration lower than 200.0 mg·L^{-1}.

As observed from Figure 7, there were no noticeable increases in the q_e or RE caused by increasing the temperature from 20 °C to 40 °C for the adsorption of MB on MS_{DW}. On the other hand, with the addition of MS_{AP}, the RE of MB increased considerably as the temperature increased, especially when the initial concentration reached 100 mg·L^{-1}. The increase could be because the mobility of dye molecules was higher with increasing temperature, and because the solution viscosity of the adsorbent particles was lower. MS_{AP} presented a superior adsorption capacity in comparison to MS_{DW} under the fixed conditions. It was obvious that the better adsorbent properties enhanced the possibility of MB molecules' enrichment on the active binding sites. Specifically, the maximum RE of MB by both MS_{DW} and MS_{AP} occurred at the initial MB concentration of 25 mg·L^{-1} and achieved 62.42% and 99.67%, respectively.

The Langmuir and Freundlich isotherm models were used to analyze the adsorption isotherms of the MB. The Langmuir isotherm model is expressed as Equation (3), and its linear form is expressed as Equation (4) (Rashed *et al.* 2016):

$$q_t = \frac{K_L q_{max} C_e}{1 + K_L C_e} \tag{3}$$

$$\frac{C_e}{q_t} = \frac{1}{K_L q_{max}} + \frac{C_e}{q_{max}} \tag{4}$$

where K_L is the Langmuir adsorption constant related to adsorption energy and the affinity of binding sites; C_e is the equilibrium concentration in the solution, mg L^{-1}; and q_{max} is the maximum adsorption capacity of MS_x, mg g^{-1}.

The Freundlich isotherm model assumes that all adsorption sites in the MS_x are heterogeneous and that the adsorption mechanism is multilayer adsorption. The Freundlich isotherm model is expressed as Equation (5):

$$q_t = K_F C_e^{1/n} \tag{5}$$

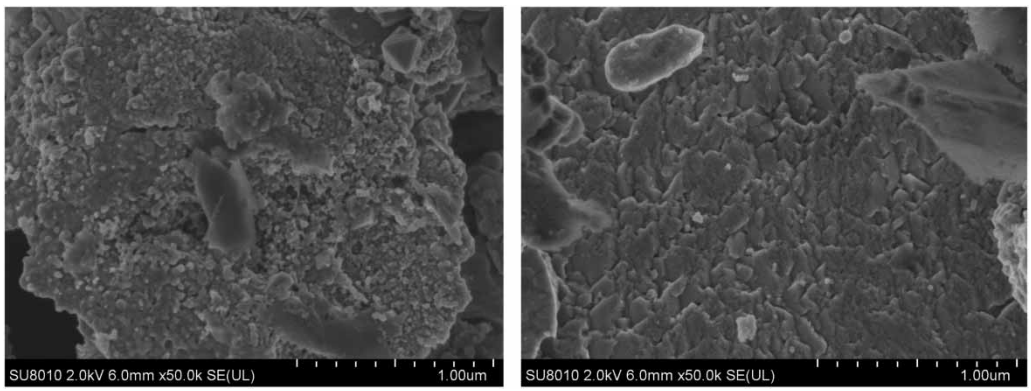

Figure 6 | SEM images for MS_{AP} before and after MB biosorption.

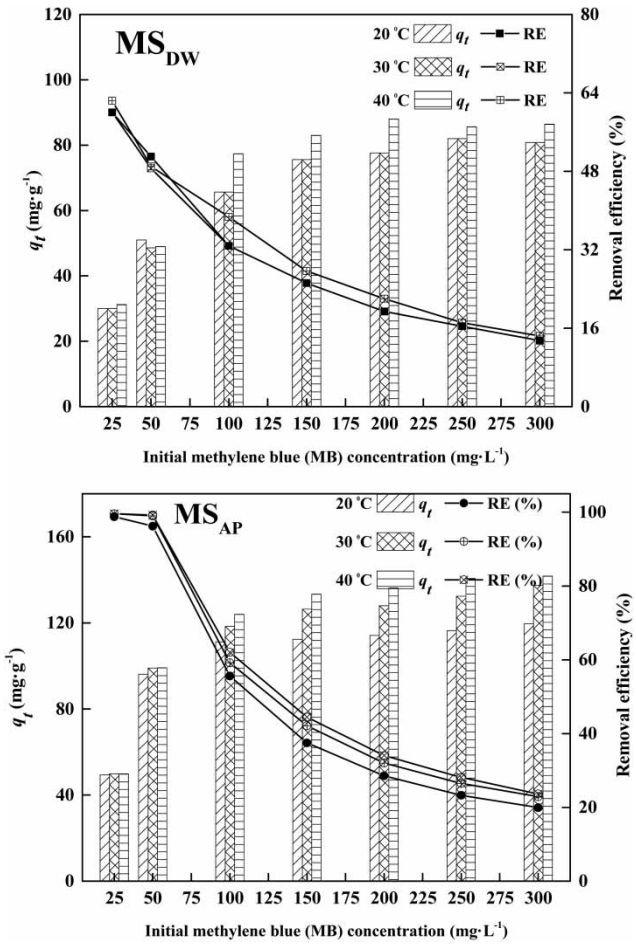

Figure 7 | Effects of initial concentration and constant temperature on the adsorption performance.

where n is the heterogeneity factor and K_F is the Freundlich constant (mg g^{-1}). The linear form of the Freundlich equation is expressed as Equation (6):

$$lnq_t = lnK_F + \frac{1}{n} lnC_e \quad (6)$$

The n is related to the adsorption intensity or surface heterogeneity. A lower value of n indicates a lesser heterogeneity. Generally, n is between 1 and 10, which points to favorable adsorption (Miraboutalebi *et al.* 2017).

All of the thermodynamic parameters for the Langmuir model and Freundlich models are shown in Table 3. The adsorption was fitted well by the Langmuir isotherm model. All of the correlation coefficient values (R^2) for the Langmuir model were greater than 0.99. The maximum adsorption capacity (q_{max}) of MS_{AP} was reached at 30 °C, the value for this was 149.05 mg g^{-1}. K_L for MS_{DW} remained constant while K_L for MS_{AP} increased with the increasing temperature; thus, the affinity between MB and MS_{AP} increased with increasing temperature.

The effects of contact time and adsorbent dosages on adsorption

The effects of contact time on the adsorption of MB by both MS_{DW} and MS_{AP} at three adsorbent dosages were studied; the temperature was 20 °C, and the initial concentration of MB was 50 mg·L^{-1}. It can be seen from Figure 8 that the adsorption process of MB was initially quite rapid and thereafter progressively slowed down until it reached equilibrium in the later stage. This phenomenon could be explained by the saturation of the existing available active sites on adsorbents with prolonged duration and the electrostatic repulsion between the increasingly crowded cationic MB molecules that had already been adsorbed onto the adsorbent and those remaining in solution (Rekha *et al.* 2017). The adsorption of MB by MS_{AP} reached equilibrium within 5 min at all studied dosages, whereas in the case of the unmodified MS_{DW}, the shortest equilibrium time was 3 min with a dosage of 0.25 g·L^{-1}.

As shown in Figure 8, similar effects of adsorbent dosages on MB adsorption were observed for both MS_{DW} and MS_{AP}. That is, the RE of MB by MS_{DW} and MS_{AP}

Table 3 | Thermodynamic parameters for the Langmuir and Freundlich models

		Langmuir model			Freundlich model		
Adsorbents	**Temperature °C**	**R^2**	**q_{max}**	**K_L**	**R^2**	**n**	**K_F**
MS_{DW}	20	0.9991	87.7193	0.0521	0.9253	3.4095	2.4101
	30	0.9991	88.4956	0.0488	0.9430	3.3113	2.3149
	40	0.9973	93.4579	0.0591	0.9046	3.1928	2.3954
MS_{AP}	20	0.9991	142.8571	0.2925	0.8263	9.2081	59.4852
	30	0.9991	149.0476	0.3665	0.7984	9.2251	31.4164
	40	0.9980	135.1351	0.4221	0.8181	9.6805	53.3721

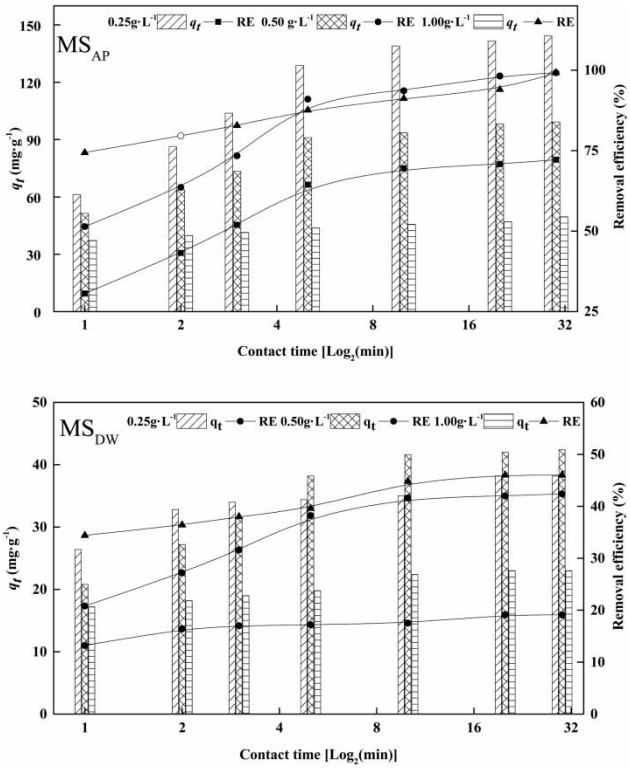

Figure 8 | Effects of contact time on adsorption at different adsorbent dosages.

presents an increasing trend, and yet q_t displayed a decreasing trend with increasing adsorbent dosage over a fixed contact time, indicating that the adsorption process involved was highly dependent on the adsorbent dosages.

The adsorption kinetics studies are of practical significance to provide important information for design and analysis in the adsorption process of dye molecules onto adsorbents. Multiple studies for the two typical kinetics models have revealed that the pseudo second order model is suitable for the adsorption periods (Franco *et al.* 2017). Thus, the pseudo second order model with the linearized form was employed to describe the adsorption mechanism of MB by MS_{DW} and MS_{AP}, and the equation is represented as Equation (7):

$$\frac{t}{q_t} = \frac{1}{k_2 q_e^2} + \frac{t}{q_e} = \frac{1}{h_0} + \frac{t}{q_e} \tag{7}$$

where k_2 is the second-order rate constants for the adsorption process, g·mg^{-1}·min^{-1}; t is the reaction time, min; q_e is the equilibrium adsorption capacity amount of dye of the adsorbent, mg·g^{-1}; and h_o represents the initial adsorption rate, mg·g^{-1}·min^{-1}.

The fitting curves as a function of contact time are shown in Figure 9; the adsorption fits well with the pseudo second order model. The values of k_2, q_e, and R^2, along with the residual root mean square error (RMSE) and the sum of the squares of the errors (SSE), are tabulated in Table 5. It was clearly confirmed that the pseudo second order model provided better prediction for the adsorption kinetics data, together with the higher R^2 and smaller error function values (RMSE and SSE).

As shown in Table 4, the second-order rate constants (k_2) and the initial adsorption rate (h_0) increased with increasing adsorbent dosages. Under the given experimental conditions, MS_{DW} required less time to reach equilibrium than MS_{AP}, likely because the q_e for MS_{AP} was 2.1 to 2.8 times that for MS_{DW}.

Table 5 gives the comparative summary of the maximum adsorption rate constants of various adsorbents towards dyes including the MB from aqueous solution; it can be

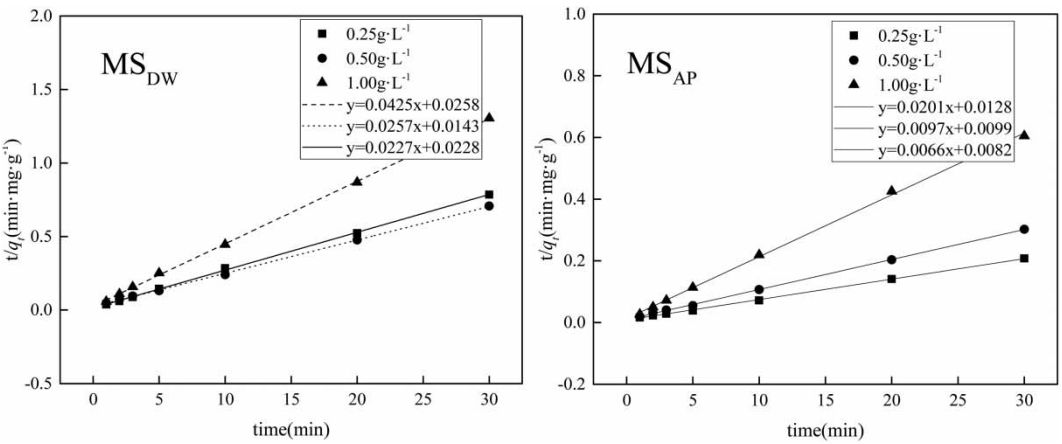

Figure 9 | The pseudo-second-order model for the adsorption process.

Table 4 | Adsorption kinetics parameters for MB onto the MS_{DW} and MS_{AP}

Materials	Dosage (g/L)	k_2	h_0	q_e	R^2	RMSE	ARE(%)
MS_{DW}	5	0.0462	69.9301	38.9105	0.9994	0.263	1.889
	10	0.0226	43.8596	44.0529	0.9995	0.210	2.946
	20	0.0700	38.7597	23.5294	0.9997	0.065	0.424
MS_{AP}	5	0.0425	121.9512	151.5152	0.9997	0.195	1.306
	10	0.0760	101.0101	103.0928	0.9998	0.149	0.904
	20	0.0525	78.1250	49.7512	0.9999	0.011	0.203

Table 5 | Comparative summary of the maximum adsorption rate constants of various adsorbents towards dyes from aqueous solution

				Experimental conditions		
Adsorbents	Modifiers	q_{max}·mg·g^{-1}	k_2 (g·mg^{-1}·min^{-1})	Initial concentration (mg/L)	Temperature (°C)/pH	References
Biochar	Citric acid	108	0.00638	15	30/5	Sun *et al.* (2015)
Kaolinite	Sulfuric acid	101	0.023	100	22/7	Gao (2016)
Chitosan/sepiolite composite	Epichlorohydrin	41	0.00385	25	30	Marrakchi *et al.* (2016)
MIL-101-SO_3H	2-sulfoterephthalic acid	/	0.00041	200		Luo *et al.* (2017)
Nanohydrogel	Starch/Poly(alginic acid-cl-acrylamide)	31.24	/			Sharma *et al.* (2017)
Masau stones	None	65.1	/		60	Albadarin *et al.* (2017)
Nano- Fe_3O_4	Trisodium citrate	435	/	10	25	Alqadami *et al.* (2016)
MS_{AP}	$(NH_4)_2S_2O_8$	149	0.0525	50	30/11	This study

seen from the table that the rate constant of MS_{AP} reached 0.05 g·mg^{-1}·min^{-1}, which was far greater than those of the other modified adsorbents. Furthermore, the q_{max} of MS_{AP} is average among the materials listed. The better adsorption of MB on MS_{AP} occurred due to the H-bond and electrostatic interactions. On the other hand, the adsorbents being studied included synthetic materials and minerals, while the sludge was the byproduct of the sewage treatment plant. Thus, the use of the MS_{AP} for MB is more promising since the sewage sludge could be reused.

CONCLUSION

Modified PS has been studied for MB removal in this manuscript, and chemical modification through loading of inorganic ions, chemical grafting of new function groups, oxidative modification and ultrasonic (US) or microwave (MW) energy assisted modification was used for the modifications. Among the 19 modified adsorbents, the RE of the $(NH_4)_2S_2O_8$ modified MS_{AP} was 1.2 to 4.4 times of the other types of MS_x. The preferable and superior adsorption ability of MS_{AP} was due to its characteristic features, that is, abundant reactive sites, large pore volume, and high surface area. The comprehensive influences of various parameters, including the solution pH, initial concentration, adsorbent dosage, temperature, and contact time have been tested. The adsorption characteristics of MS_{AP} were also compared with those of the MS_{DW} which had not been modified. A pH of 10 was preferred for a lower protonation level and improved electrostatic attraction. From the thermodynamic properties investigation, the isothermal adsorption model for the adsorption was better fitted by the Langmuir model, for which the R^2 values were greater than 0.99. The q_{max} of MS_{AP} was 149.05 mg g^{-1}; furthermore, the affinity of MB and MS_{AP} prefers a higher temperature. The adsorption kinetics fit the pseudo second order model; when the addition of MS_{AP} was 1 g·L^{-1}, the rate constant reached 0.05 g·mg^{-1}·min^{-1}, which was far greater than that of the

other modified adsorbents. Furthermore, the q_{max} of MS_{AP} is average among the materials listed.

ACKNOWLEDGEMENTS

This work was supported by the National Natural Science Foundation of China Youth Fund (No. 41503116), Guangzhou Science and Technology Program (No. 201607020003), Guangdong Provincial Science and Technology Program (No. 2014B090901040, 2015B020237003).

REFERENCES

Albadarin, A. B., Charara, M., Tarboush, B. J., Ahmad, M. N. M., Kurniawan, T. A., Naushad, M., Walker, G. M. & Chirangano, M. 2017 Mechanism analysis of tartrazine biosorption onto masau stones; a low cost by-product from semi-arid regions. *Journal of Molecular Liquids* **242**, 478–483.

Alqadami, A. A., Naushad, M., Abdalla, M. A., Khan, M. R. & Alothman, Z. A. 2016 Adsorptive removal of toxic dye using Fe_3O_4-TSC nanocomposite: equilibrium, kinetic, and thermodynamic studies. *Journal of Chemical & Engineering Date* **61**, 3806–3813.

Banaei, A., Ebrahimi, S., Vojoudi, H., Karimi, S. & Pourbasheer, E. 2017 Adsorption equilibrium and thermodynamics of anionic reactive dyes from aqueous solutions by using a new modified silica gel with 2,2'-(pentane-1,5-diylbis(oxy))dibenzaldehyde. *Chemical Engineering Research and Design* **123**, 50–62.

Chen, T., Zhou, Z., Han, R., Meng, R., Wang, H. & Lu, W. 2015 Adsorption of cadmium by biochar derived from municipal sewage sludge: impact factors and adsorption mechanism. *Chemosphere* **134**, 286–293.

Dahri, M. K., Kooh, M. R. R. & Lim, L. B. L. 2015 Application of Casuarina equisetifolia needle for the removal of methylene blue and malachite green dyes from aqueous solution. *Alexandria Engineering Journal* **54** (4), 1253–1263.

Fan, S., Tang, J., Wang, Y., Li, H., Zhang, H., Tang, J., Wang, Z. & Li, X. 2016 Biochar prepared from co-pyrolysis of municipal sewage sludge and tea waste for the adsorption of methylene blue from aqueous solutions: kinetics, isotherm, thermodynamic and mechanism. *Journal of Molecular Liquids* **220**, 432–441.

Ferreira, C. I., Calisto, V., Otero, M., Nadais, H. & Esteves, V. I. 2017 Removal of tricaine methanesulfonate from aquaculture wastewater by adsorption onto pyrolysed paper mill sludge. *Chemosphere* **168**, 139–146.

Franco, D. S. P., Cunha, J. M., Dortzbacher, G. F. & Dotto, G. L. 2017 Adsorption of Co (II) from aqueous solutions onto rice husk modified by ultrasound assisted and supercritical technologies. *Process Safety and Environmental Protection* **109**, 55–62.

Gao, W., Zhao, S., Wu, H., Deligeer, W. & Asuha, S. 2016 Direct acid activation of kaolinite and its effects on the adsorption of methylene blue. *Applied Clay Science* **126**, 98–106.

Jung, K. W., Choi, B. H., Hwang, M. J., Jeong, T. U. & Ahn, K. H. 2016 Fabrication of granular activated carbons derived from spent coffee grounds by entrapment in calcium alginate beads for adsorption of acid orange 7 and methylene blue. *Bioresource Technology* **219**, 185–195.

Luo, X. P., Fu, S. Y., Du, Y. M., Guo, J. Z. & Li, B. 2017 Adsorption of methylene blue and malachite green from aqueous solution by sulfonic acid group modified MIL-101. *Microporous and Mesoporous Materials* **237**, 268–274.

Manna, S., Saha, P., Roy, D., Gopakumar, D. & Thomas, S. 2017 Rapid methylene blue adsorption using modified lignocellulosic materials. *Process Safety and Environmental Protection* **107**, 346–356.

Marrakchi, F., Khanday, W. A., Asif, M. & Hameed, B. H. 2016 Cross-linked chitosan/sepiolite composite for the adsorption of methylene blue and reactive orange 16. *International Journal of Biological Macromolecules* **93**, 1231–1239.

Miraboutalebi, S. M., Nikouzad, S. K., Peydayesh, M., Allahgholi, N., Vafajoo, L. & Mckay, G. 2017 Methylene blue adsorption via maize silk powder: kinetic, equilibrium, thermodynamic studies and residual error analysis. *Process Safety and Environmental Protection* **106**, 191–202.

Qin, H. D., Xiao, R., Zhang, R. H. & Chen, J. 2018 Efficient adsorption of benzoic acid from aqueous solution by nitrogen-containing activated carbon. *Water Science & Technology* **2017** (3), 686–694.

Rashed, M. N., El-Daim, M. A., Taher, E. & Fadlalla, S. M. M. 2016 Adsorption of methylene blue using modified adsorbents from drinking water treatment sludge. *Water Science & Technology* **74**, 1885–1898.

Rekha, K. G., Radhika, R., Jayalatha, T., Jacob, S., Rajeev, R., George, B. K. & Anjali, B. R. 2017 Removal of perchlorate from drinking water using granular activated carbon modified by acidic functional group: adsorption kinetics and equilibrium studies. *Process Safety and Environmental Protection* **109**, 158–171.

Sharma, G., Naushad, M., Kumar, A., Rana, S., Sharma, S., Bhatnagar, A., Stadler, F., Ghfar, A. A. & Khan, M. R. 2017 Efficient removal of coomassie brilliant blue R-250 dye using starch/poly(alginic acid-cl-acrylamide) nanohydrogel. *Process Safety and Environmental Protection* **109**, 301–310.

Shim, J., Shea, P. J. & Oh, B. T. 2014 Stabilization of heavy metals in mining site soil with silica extracted from corn cob. *Water Air and Soil Pollution* **225**, 1–12.

Sun, L., Chen, D. M., Wan, S. G. & Yu, Z. B. 2015 Performance, kinetics, and equilibrium of methylene blue adsorption on biochar derived from eucalyptus saw dust modified with citric, tartaric, and acetic acids. *Bioresource Technology* **198**, 300–308.

Zhang, B., Dong, Z., Sun, D., Wu, T. & Li, Y. 2017 Enhanced adsorption capacity of dyes by surfactant-modified layered double hydroxides from aqueous solution. *Journal of Industrial and Engineering Chemistry* **49**, 208–218.

First received 4 April 2018; accepted in revised form 27 July 2018. Available online 14 August 2018